

doi:10.15199/48.2017.01.09

A single-switch class E voltage-source inverter for induction heating - influence of the parameters of the resonant circuit elements on its performance at optimal control

Abstract. The object of the article is a single-switch transistor inverter for induction heating operating optimally in class E. Results of measurements carried out in a novel inverter model at a few values of resonant capacitance for a few types of charge are presented. They are in a good accordance with the conclusions resulting from the theoretical analysis of the inverter.

Streszczenie Przedmiotem artykułu jest jednołącznikowy falownik tranzystorowy do nagrzewania indukcyjnego pracujący optymalnie w klasie E. W artykule przedstawiono wyniki pomiarów zrealizowanych przy kilku wartościach pojemności rezonansowej dla kilku rodzajów wsadu w wykonanym oryginalnym modelu falownika. Potwierdzają one wnioski wynikające z analizy teoretycznej falownika. (Jednołącznikowy falownik napięciowy klasy E do nagrzewania indukcyjnego - wpływ wartości elementów obwodu rezonansowego na parametry jego pracy przy sterowaniu optymalnym)

Keywords: single-switch topology, ZVS, class E inverters, induction heating

Słowa kluczowe: układ jednołącznikowy, ZVS, falowniki klasy E, nagrzewanie indukcyjne

Introduction

A group of inverters used in induction heating are single-switch inverters. They are used at low powers, usually up to (2÷4) kW. One of them is a class E voltage-source inverter shown in Figure 1. This inverter topology is presented in literature [1-3], especially in connection with its application in induction cookers, operating usually in the frequency range of (20÷50) kHz. Reference [4] contains an analysis of the inverter optimal operation, at which the switching losses are the lowest. Maintaining such switching conditions makes it possible to operate the inverter at frequencies of several hundred kilohertz. A concept of the inverter's control and an assessment of its efficiency for different load parameters are presented in [5, 6].

This article presents selected results of measurements of an experimental setup of the discussed inverter and their comparison with theoretical calculations.

Types of the inverter's operation

The inverter (Fig. 1a) is supplied from a DC voltage source U_d . Resistance R_0 and inductance L_0 represent the inductor-charge system. Capacitor C is selected in a way to obtain the required frequency of oscillations. A MOSFET transistor is used as the power electronic switch.

Each switching cycle in steady-state conditions can be divided into two operating modes. In mode I (time interval T_1 in Figure 1b) switch S (transistor T , or diode D first and next the transistor T) conducts electrical current. Current i_s rises exponentially, while the voltage u_c across C and R_0L_0 is practically constant and equal to U_d . After the switch is off, mode II begins and an oscillation occurs in the R_0L_0C circuit.

If resistance R_0 is sufficiently low, voltage u_c reaches the magnitude of supply voltage U_d , which means the end of mode II and the beginning of the next switching cycle. If, additionally, maximum voltage u_c in mode II equals U_d , the next switching cycle will start with zero switch current i_s (there is no diode D current, as can be seen in Figure 1b). Therefore, the switch S is turned on at zero voltage (ZVS) and zero current (ZCS). The turn-off occurs at zero voltage. The switching losses are the lowest and this type of the inverter operation is termed optimal operation.

The other possible operating types of the inverter are suboptimum and non-optimum operation. They are briefly described in [4, 6].

Optimal operation of the inverter – general dependencies

The inverter optimal operation is only possible if the quality factor Q (1) of the series resonant circuit R_0L_0C is sufficiently high ($Q > ca 2.6085$) [4, 6]. For lower values of Q voltage u_T never reaches U_d in mode II and a soft turn-on of the transistor is not possible. For preset circuit parameters R_0L_0C , which determine the value of Q , the inverter optimal operation is only possible at unique, strictly determined values of angular switching frequency $\omega_s = 2\pi f_s$ and conduction time T_1 of the transistor. The relationships between the normalized switching angular frequency $\omega_{sn} = \omega_s / \omega_0$, normalized transistor conduction time $D = T_1 / T_s$ (Fig. 1b) and quality factor Q are shown in Figure 2a, where [4]:

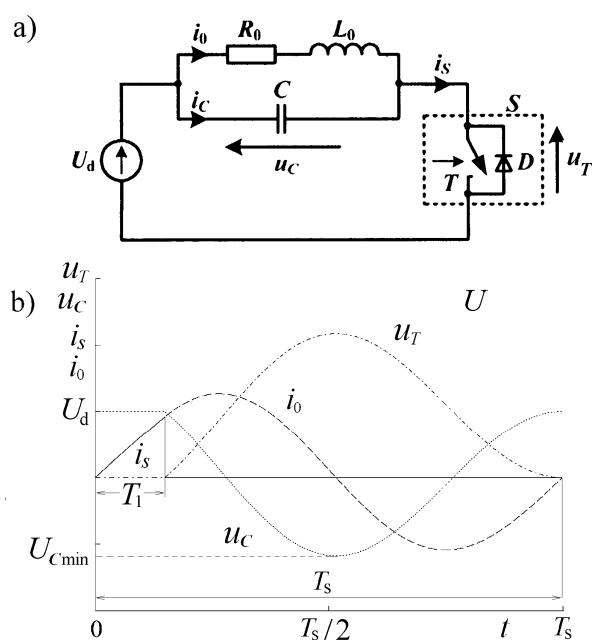


Fig. 1. Class E single-switch voltage-source inverter: a) basic circuit diagram; b) example of voltage and current waveforms at optimal operation

$$(1) \quad Q = \frac{\sqrt{L_0}}{R_0}; \quad \alpha_{0n} = \frac{R_0}{2\omega_0 L_0};$$

$$Z_0 = \sqrt{\frac{L_0}{C}}; \quad \omega_0 = \sqrt{\frac{1}{L_0 C} - \left(\frac{R_0}{2L_0}\right)^2}$$

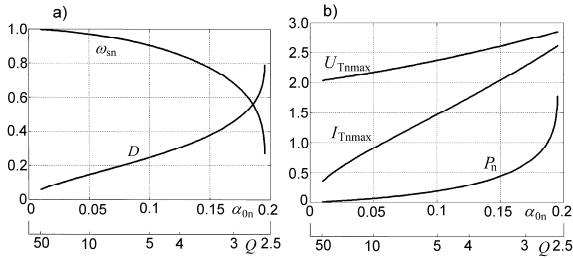


Fig. 2. Dependencies for optimal operation of the inverter: a) relationships between D , ω_{sn} and α_{0n} (Q), b) normalized maximum transistor current, maximum transistor voltage and inverter power [4]

Normalized values of the maximum transistor current I_{Tnmax} , maximum voltage U_{Tnmax} across the transistor and inverter power P_n

$$(2) \quad I_{Tnmax} = I_{Tmax} \frac{Z_0}{U_d}; \quad U_{Tnmax} = \frac{U_{Tmax}}{U_d}; \quad P_n = P \frac{Z_0}{U_d^2}$$

versus quality factor Q are shown in Figure 2b [4]. The equations are valid for steady state condition on the assumption that all the elements are ideal and the supply voltage U_d stays constant in one switching cycle.

Experimental results

Results of investigations of an original experimental setup of the inverter (Table 1) are presented in this chapter. A single heating inductor has been used for a few types of charge at a few values of the resonant capacitance.

Table 1. Parameters of the experimental setup (Fig. 3)

| Parameter | Value |
|----------------------------------------------------|----------------------------------------------------------------------------------------------------------------------------------------------------------------------|
| Input voltage, V | up to 60 |
| Power, W | up to 800 |
| Capacitor C , nF | 141, 235, 329 and 423 |
| Semiconductor switch (two transistors in parallel) | MOSFET IRFP260N $R_{DS(on)} = 40 \text{ m}\Omega$ |
| Inductor | 10 turns of $\varnothing 4 \text{ mm}$ copper pipe, |
| Load | steel rod, $\varnothing 4 \text{ mm}$, magnetic; steel rod, $\varnothing 8 \text{ mm}$, magnetic; steel rod, $\varnothing 10 \text{ mm}$, slightly magnetic |

One of the stages of the investigations was determination of the values of the resistance and the inductance of the equivalent inductor-charge system for each measured case. To this end, a series of measurements of the damping in the resonant circuit was made. The transistor gate pulse generator was reconfigured to a single pulse generator. Next, free oscillations were generated and, based on the registered waveforms (measurement of consecutive peak values I_{01m} and I_{02m} of the load current i_0 and angular frequency $\omega_0 = 2\pi f_0$ of the free oscillations), the values of resistance R_0 and inductance L_0 were determined using the following relations:

$$(3) \quad L_0 = \frac{1}{C(\omega_0^2 + \beta^2)}; \quad R_0 = 2\beta L_0; \quad \beta = \ln\left(\frac{I_{01m}}{I_{02m}}\right) f_0.$$



Fig. 3. Investigated model of the inverter

These measurements were made for a few different loads. Some of them were: a slightly magnetic rod of diameter 10 mm and magnetic rods of diameters 4 mm and 8 mm. For each load, capacitors 141 nF, 235 nF, 329 nF and 423 nF were used consecutively. These values of the capacitances were obtained by paralleling an appropriate number of 47 nF capacitors. The measurements results and the values of L_0 , R_0 and Q calculated on their basis for $C = 141 \text{ nF}$ and various loads are shown in Table 2.

Next, measurements at optimal operation of the inverter were made for each combination of the load and the capacitance. This was possible due to using an original control system, which was able to choose the optimal operating point in each case. Tables 3 and 4 present the measurements results for magnetic loads of diameters 4 mm and 8 mm, respectively, at four different values of the capacitance.

Comparison of results in Tables 3 and 4 shows that the increase of the load diameter from 4 mm to 8 mm resulted in:

- increase of resistance R_0 and decrease of inductance L_0 and quality factor Q ,
- increase of frequency f_0 ,
- decrease of switching frequency f_s at optimal operation, as at decrease of Q the ratio f_s/f_0 decreases (Fig. 2a),
- an increase of duty cycle D , as at decrease of Q the control system increases D to compensate for higher energy produced in the charge and maintain the optimal operation.

Figure 4 shows a graphical representation of selected results of the inverter measurements after rescaling. Due to the dependence of the inverter current on capacitance C and a limited current capacity of the supply unit used in the measurements (Sorensen DCR300 – 9B, $I_{max} = 10 \text{ A}$), the supply voltage U_d magnitude was varied (Tab. 2 - Tab. 4). To have a possibility of comparing the currents, voltages and powers for different cases, these quantities were rescaled to a reference supply voltage $U_{d-ref} = 50 \text{ V}$. Examples of rescaled measurements results for the magnetic charge of diameter 8 mm are shown in Table 5.

It results from a comparison of the data in Figure 4 and Table 5 with the graphs in Figure 2b that the general trends in the changes of these parameters are consistent.

At a preset inductor-charge system, an increase of the capacitance C involves a decrease of quality factor Q (1) and frequency f_s . The latter is caused both: by lowering of the natural frequency ω_0 of the oscillations in the $R_0 L_0 C$ circuit and by a decrease of the required ratio ω_s/ω_0 (Fig. 2a).

Table 2. Results of measurements for resonant capacitance $C = 141$ nF at three different loads: 1 – slightly magnetic load $\varnothing 10$ mm, 2 – magnetic load $\varnothing 4$ mm, 3 – magnetic load $\varnothing 8$ mm [6, 7]

| Load | Free oscillations | | | | Optimal operation | | | | | |
|------|-------------------|------------------|---------------------|------|-------------------|--------------|-------|-----------------|-----------------|---------------|
| | f_0 kHz | L_0 μ H | R_0 m Ω | Q | U_d V | f_s kHz | D | U_{Tmax} V | I_{Tmax} A | P_{in} W |
| 1 | 775.2 | 0.299 | 99.59 | 14.6 | 93.0 | 751.9 | 0.132 | 215 | 47.5 | 334.8 |
| 2 | 636.9 | 0.437 | 407.6 | 4.32 | 69.0 | 565.0 | 0.283 | 175 | 52.5 | 586.5 |
| 3 | 689.7 | 0.371 | 437.1 | 3.71 | 29.0 | 520.8 | 0.391 | 86 | 37.5 | 275.5 |

Table 3. Results of measurements for magnetic load $\varnothing 4$ mm at four different values of resonant capacitance C [6, 7]

| C nF | Free oscillations | | | | Optimal operation | | | | | | | |
|-----------|-------------------|------------------|---------------------|------|-------------------|--------------|------------------|-------|-----------------|-----------------|---------------|--|
| | f_0 kHz | L_0 μ H | R_0 m Ω | Q | U_d V | f_s kHz | T_1 μ s | D | U_{Tmax} V | I_{Tmax} A | P_{in} W | |
| 141 | 636.9 | 0.437 | 407.6 | 4.32 | 69.0 | 565.0 | 0.50 | 0.283 | 175 | 52.5 | 587 | |
| 235 | 495.0 | 0.432 | 352.9 | 3.84 | 68.0 | 448.4 | 0.65 | 0.292 | 165 | 57.5 | 578 | |
| 329 | 420.2 | 0.427 | 334.2 | 3.41 | 33.6 | 359.7 | 0.85 | 0.306 | 89 | 45.0 | 252 | |
| 423 | 365.0 | 0.439 | 315.7 | 3.23 | 33.6 | 318.5 | 0.95 | 0.303 | 88 | 48.8 | 279 | |

Table 4. Results of measurements for magnetic load $\varnothing 8$ mm at four different values of resonant capacitance C [6, 7]

| C nF | Free oscillations | | | | Optimal operation | | | | | | | |
|-----------|-------------------|------------------|---------------------|------|-------------------|--------------|------------------|-------|-----------------|-----------------|---------------|--|
| | f_0 kHz | L_0 μ H | R_0 m Ω | Q | U_d V | f_s kHz | T_1 μ s | D | U_{Tmax} V | I_{Tmax} A | P_{in} W | |
| 141 | 689.7 | 0.371 | 437.1 | 3.71 | 29.0 | 520.8 | 0.75 | 0.391 | 86 | 37.5 | 276 | |
| 235 | 523.6 | 0.384 | 391.3 | 3.27 | 24.0 | 403.2 | 1.00 | 0.403 | 71 | 41.3 | 216 | |
| 329 | 442.5 | 0.382 | 371.0 | 2.90 | 15.4 | 301.2 | 1.45 | 0.437 | 47 | 31.3 | 145 | |
| 423 | 384.6 | 0.391 | 352.8 | 2.73 | 15.7 | 274.7 | 1.50 | 0.412 | 49 | 35.0 | 144 | |

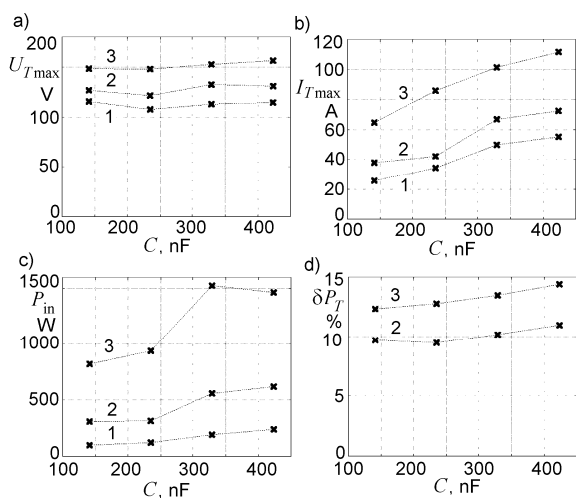


Fig. 4. Selected results of measurements for 4 values of capacitance C and 3 types of load at optimal operation: a) maximum voltage across the switch (rescaled), b) maximum switch current (rescaled), c) inverter input power (rescaled), d) normalized losses in the switch; 1 – slightly magnetic rod $\varnothing 10$ mm, 2 – magnetic steel rod $\varnothing 4$ mm, 3 – magnetic steel rod $\varnothing 8$ mm [7]

An increase of the damping factor involves an increase of the energy generated in the inductor-charge

system in mode II. To ensure optimal operation, the energy stored in the inductor L at the end of mode I has also to increase. Therefore, the following quantities increase as well: transistor conduction time T_1 , maximum transistor current I_{Tmax} , maximum voltage U_{Cmax} across the transistor and the inverter power.

Table 5. Selected results of measurements after rescaling to $U_{d-ref} = 50$ V - magnetic steel rod $\varnothing 8$ mm at four different capacitances C of the resonant circuit [7]

| C , nF | U_d , V | U_{Tmax} , V | I_{Tmax} , A | P_{in} , W |
|----------|-----------|----------------|----------------|--------------|
| 141 | 50 | 148 | 64.7 | 819 |
| 235 | | 148 | 85.9 | 938 |
| 329 | | 153 | 101.5 | 1526 |
| 423 | | 156 | 111.5 | 1465 |

An original pulse generator controlling the switch S (two MOSFETs IRFP260N connected in parallel) was used in the constructed model of the inverter. The available pulse width was in the range: (84 ÷ 1480) ns. This range was a result of design assumptions, regarding rather smaller size loads (lower damping). Further increasing the width of the pulses by the regulator used in the control unit of the inverter would result in an increase of the average current of the transistor i_T over the permissible value. This would expose it to the overcurrent and, consequently, could lead to thermal damage. A possible reduction of supply voltage U_d would result in lower output power (which could be too low to heat-up the load sufficiently) but also in a sharp decrease of electrical efficiency of the inductor-charge system. This

is due to a very unfavorable ratio of voltage u_T across the conducting transistor to supply voltage U_d occurring in such situations.

Increasing capacitance C caused an increase of parasitic oscillations in transistor current i_T (Figs. 5a and 5b), especially in the case of circuits with high damping factor. A slight deviation from the optimal operating point of the inverter can be seen in Figure 5b. Due to a significant value of the parasitic inductance in the circuit, this did not result in a rapid build-up of the current. However, further increase of the damping in the oscillating circuit R_0L_0C would increase this phenomenon, causing a pronounced shift in the operating status to non-optimum operation.

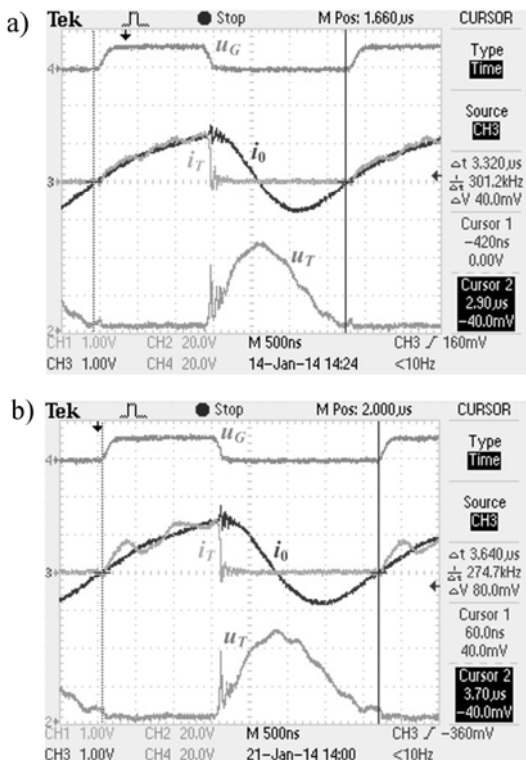


Fig. 5. Waveforms of currents and voltages in an inverter loaded with a rod of magnetic steel $\varnothing 8 \text{ mm}$ with the parameters as follows: a) $U_d = 15.4 \text{ V}$, 329 nF , b) $U_d = 15.7 \text{ V}$, 423 nF ; i_T , $i_0 - 25 \text{ A/div}$, $u_T - 20 \text{ V/div}$

The increase in the relative losses (referenced to the input power) in the transistor (Fig. 4d) with an increase in C is the result of an increase of the conduction losses in the switch (larger current i_T) and increased losses during the switch-off period (prolonged switch-off time at larger current i_T). The original control system developed in the investigated inverter model brings the inverter's operating point to optimal one for different loads; therefore there was no increase in the turn-on losses in the transistor.

Some deviations from the trend, noticeable on some graphs in Figure 4 (particularly evident for the load of magnetic steel $\varnothing 8 \text{ mm}$), result, among others, from the limited current capacity of the supply unit as well as from the aforementioned restrictions and limits of the switch control pulses generator and the switch S itself.

Another limitation of this system is the design of the inverter's high-current circuit using tracks of a printed circuit board. Despite the use of a board with a thickened

layer of copper, there was a restriction on the current density. In order to eliminate, or at least to reduce, these adverse effects, the execution of the high-current circuit using a respectively stronger active conductive layer should be considered. Shortening the length between the power source and the resonant circuit R_0L_0C would also be of big importance. These modifications of the system would also reduce the peak voltage across the switch (Figs. 5a and 5b) at its turn-off.

Conclusions

Results of investigations of a model of a single-switch class E voltage-source inverter for induction heating operating at optimal control have been presented in this paper. It was possible to carry out these measurements due to using an original control system, which was able to choose the optimal operating point in each case.

The influence of the resonant circuit capacitance and the type of the charge on the basic properties of the inverter has been discussed. There is a good accordance between the theoretical and experimental results. In the case of some differences, the possible reasons were given and some ways of improving the inverter performance were shown.

Authors: dr inż. Aleksander Skala, AGH-Akademia Górniczo-Hutnicza, Katedra Energoelektroniki i Automatyki Systemów Przetwarzania Energii, al. A. Mickiewicza 30, 30-059 Kraków, E-mail: aleksander.skala@agh.edu.pl; dr inż. Zbigniew Waradzyn, AGH-Akademia Górniczo-Hutnicza, Katedra Energoelektroniki i Automatyki Systemów Przetwarzania Energii, al. A. Mickiewicza 30, 30-059 Kraków, E-mail: waradzyn@agh.edu.pl

REFERENCES

- [1] Omori H., Yamashita H., Nakaoka M., Maruhashi T.: A Novel Type Induction-Heating Single-Ended Resonant Inverter Using New Bipolar Darlington-Transistor. *IEEE Power Electronics Specialist Conference Rec.*, 1985, Vol. 1, s. 590-599.
- [2] Llorente S., Monterde F., Burdío J.M., Acero J.: A Comparative Study of Resonant Inverter Topologies Used in Induction Cookers, *Applied Power Electronics Conference and Exposition, APEC 2002*, Vol. 2, s. 1168-1174.
- [3] Saoudi M., Puyal D.; Bernal C.; Antón, D.; Mediano, A.: Induction Cooking Systems with Single Switch Inverter Using New Driving Techniques, *Industrial Electronics (ISIE)*, 2010 *IEEE International Symposium on*, vol. no. 4-7 July 2010, s.878-883.
- [4] Waradzyn Z., Skala A., Świątek B., Klempka R., Kieroński R.: ZVS single-switch inverter for induction heating – optimum operation. *Przegląd Elektrotechniczny*, R. 90 nr 2/2014, s. 32–35.
- [5] Skala A., Waradzyn Z.: Determination of Efficiency in a Single-Switch Class E ZVS-1S Quasi-Resonant Inverter in Application for Induction Heating. *Przegląd Elektrotechniczny*, R. 92 nr 3/2016, s. 99–102.
- [6] Skala A.: Falownik ZVS-1S w zastosowaniu do nagrzewania indukcyjnego. *Rozprawa doktorska*. AGH Kraków, 2014 (in Polish).
- [7] Skala A., Waradzyn Z.: Wpływ wartości elementów obwodu oscylacyjnego jednołącznikowego falownika napięciowego klasy E do nagrzewania indukcyjnego na parametry jego pracy przy sterowaniu optymalnym. *Monografie, studia, rozprawy*. M69. *Procesy elektrotechnologiczne – modelowanie i sterowanie*. Politechnika Świętokrzyska 2015, Rozdz. 2.3, s. 89-100 (in Polish).